



RESEARCH ARTICLE

10.1029/2025JH000910

Special Collection:

Advanced machine learning in solid earth geoscience

Key Points:

- Analytical methods, including sliding-window detection and cubic fitting, enable identification of instant and transitional change points
- ChangePointCNN-GNSS optimizes parameters to detect change points and selects the longest change-point-free segment for site velocity
- Site velocities for ~14,600 global GNSS stations, supporting global and regional reference frames and advancing broad geoscience studies

Correspondence to:G. Wang,
gwang@uh.edu**Citation:**

Wang, G., Bao, Y., Zhang, S., Huang, G., & Hu, X. (2025). ChangePointCNN-GNSS: An AI model for assessing change points and optimizing site velocity estimation from global GNSS data. *Journal of Geophysical Research: Machine Learning and Computation*, 2, e2025JH000910. <https://doi.org/10.1029/2025JH000910>

Received 19 JUL 2025

Accepted 18 OCT 2025

Author Contributions:

Conceptualization: Guoquan Wang, Yan Bao

Formal analysis: Guoquan Wang, Guanwen Huang, Xie Hu

Methodology: Guoquan Wang, Yan Bao, Shuangcheng Zhang

Writing – review & editing:

Guoquan Wang, Yan Bao, Shuangcheng Zhang, Guanwen Huang, Xie Hu

© 2025 The Author(s). *Journal of Geophysical Research: Machine Learning and Computation* published by Wiley Periodicals LLC on behalf of American Geophysical Union.

This is an open access article under the terms of the [Creative Commons](#)

[Attribution License](#), which permits use, distribution and reproduction in any medium, provided the original work is properly cited.

ChangePointCNN-GNSS: An AI Model for Assessing Change Points and Optimizing Site Velocity Estimation From Global GNSS Data

Guoquan Wang¹ , Yan Bao², Shuangcheng Zhang³ , Guanwen Huang³, and Xie Hu⁴

¹Department of Earth and Atmospheric Sciences, University of Houston, Houston, TX, USA, ²National Key Laboratory of Bridge Safety and Resilience, Beijing University of Technology, Beijing, China, ³School of Geology Engineering and Geomatics, Chang'an University, Xian, China, ⁴College of Urban and Environmental Sciences, Peking University, Beijing, China

Abstract Estimating long-term site velocities from Global Navigation Satellite System (GNSS)-derived daily displacement time series is vital for studying secular tectonic motions and establishing regional and global geodetic reference frames. However, this estimation is complicated by displacements caused by earthquakes, equipment changes, hydraulic head changes, and other sources, which introduce change points in GNSS time series. This study introduces a two-stage hybrid framework for automated change-point detection in GNSS time series. The framework integrates (a) analytical methods, including a sliding-window algorithm for instant change-point detection and a cubic polynomial fit for transitional change-point detection and (b) an artificial intelligence (AI) model, ChangePointCNN-GNSS, which evaluates the suitability of candidate change points for site velocity estimation and iteratively optimizes analytical parameters. Unlike prior data-driven approaches, our framework leverages an image-driven method, employing a convolutional neural network (CNN) to visually assess and select the most suitable change-point configuration for reliable site velocity estimation. Site velocities are computed from the longest change-point-free segment (minimum 4 years), processed independently for each station and direction. This integrated approach ensures robust site velocity estimation across large GNSS networks. The CNN is trained using approximately 6,000 time series plots with marked change points. Each plot is labeled as “good” if the detected change points are suitable for reliable site velocity estimation or “bad” if unsuitable. This study delivers long-term site velocities (IGS20) for approximately 14,600 permanent GNSS stations worldwide, with a 95% confidence interval below 1 mm/year, offering a foundational data set for researchers in geodesy, tectonophysics, and hazard mitigation.

Plain Language Summary Global Navigation Satellite System (GNSS) stations monitor Earth's surface displacements to estimate long-term site velocities, from which secular tectonic motions can be derived. These secular velocities are fundamental for studying plate movements and assessing geological hazards. However, displacements from earthquakes, equipment changes, or other factors introduce change points that disrupt reliable secular velocity estimates. Conventionally, change points are detected using analytical methods that require manual tuning of multiple parameters—a slow, impractical process that limits the use of vast global GNSS data. We developed a two-stage solution: first employing analytical methods to scan for potential change points, then using our artificial intelligence (AI) tool to assess their suitability for reliable velocity estimation—automatically fine-tuning parameters without human intervention. Applied to decades of GNSS records, this method delivers trustworthy site velocities with a 95% confidence interval under 1 mm/year. By combining classic math with a modern, image-based convolutional neural network (CNN), our method simplifies and improves the analysis of large GNSS data sets, offering reliable site velocities where conventional data-driven methods often fall short. All tools and data are shared, enabling others to apply and extend this innovation across Earth science and related fields.

1. Introduction

Displacement time series derived from Global Navigation Satellite System (GNSS) observations provide essential data for estimating long-term site velocities, which are commonly interpreted as secular tectonic motion trends in tectonically stable regions. These velocities are fundamental for the periodic updates of global geodetic reference frames (e.g., Altamimi et al., 2023), the development of regional crustal velocity models (e.g., Snay et al., 2025), and the establishment of regional and local-scale reference frames (e.g., Agudelo et al., 2020; Bao

et al., 2021; Blewitt et al., 2013; Wang et al., 2018). Since the mid-1990s, over 20,000 permanent GNSS stations worldwide have generated long-term records. GNSS-derived displacement time series are openly accessible through archives like UNAVCO (Herring et al., 2016) and the Nevada Geodetic Laboratory (Blewitt et al., 2018), enabling detailed studies of crustal motion and the development of numerous regional reference frames.

Site velocities are typically derived by applying linear regression to displacement time series to determine stable, secular trends. However, change points, both instant and transitional, frequently disrupt long-term GNSS time series due to various factors, such as earthquakes, equipment changes, groundwater level fluctuations, severe droughts, and undocumented events, complicating accurate site velocity estimation. Robust change-point detection is thus essential for the reliable analysis of large-scale GNSS networks (e.g., Gazeaux et al., 2013; Griffiths & Ray, 2016; Heflin et al., 2020).

Traditional methods for calculating site velocities from large GNSS data sets, such as the Median Interannual Difference Adjusted for Skewness (MIDAS) (Blewitt et al., 2016) and trajectory modeling (Bedford & Bevis, 2018; Bevis & Brown, 2014), face challenges with large global data sets involving frequent steps and gaps. MIDAS estimates site velocity by calculating linear trends from 1-year segments of the time series and selecting the median trend, but these segments may include complex earthquake signals or other natural and anthropogenic events, potentially biasing velocity estimates, particularly in tectonically active regions.

Catalog-driven physical trajectory models fit parametric functions, including linear trends, seasonal signals, and Heaviside step functions for known events like earthquakes, to the entire time series (Bevis & Brown, 2014). These models rely on prior knowledge of disruptive events from external sources, such as earthquake catalogs, GNSS site logs (documenting equipment changes and maintenance), and software update histories, to manually define change points. Data-driven trajectory modeling, such as greedy automatic signal decomposition, identifies trends and change points without predefined catalogs, offering flexibility for complex time series with unknown disruptions (Bedford & Bevis, 2018). However, for processing large global data sets, data-driven approaches face challenges, including high computational complexity due to iterative model fitting, sensitivity to noise and outliers across diverse stations, lack of geophysical interpretability for detected change points, parameter tuning difficulties for heterogeneous time series, and limited scalability in fully automated processing of large data sets.

To overcome the limitations of conventional methods, we propose a hybrid framework that integrates analytical techniques with a convolutional neural network (CNN), ChangePointCNN-GNSS. The process begins by using an analytical method to identify potential change points in a GNSS time series; however, the number of change points is highly sensitive to predefined threshold parameters. Our hybrid approach iteratively tests a range of these thresholds, generating a unique candidate set of change points for each one. The CNN model then evaluates and scores the suitability of each candidate set for long-term velocity estimation. This score is used to refine the analytical parameters, creating an optimization loop that converges on the most statistically robust change-point configuration. Finally, the longest change-point-free segment (minimum of 4 years) is selected from the optimal configuration, and a linear regression is applied to estimate the final site velocity. This integrated method enhances both the precision and automation of velocity estimation.

2. Data and Methods

2.1. Data

As of 2025, the NGL maintains a comprehensive data set of GNSS-derived daily displacement time series from over 20,000 GNSS stations worldwide (Blewitt et al., 2018). Among these, approximately 15,000 stations offer continuous records spanning at least 4 years, with a data availability threshold exceeding 70%. This ensures sufficient temporal and spatial coverage for estimating long-term site velocities directly from GNSS data, which can represent secular tectonic motion in stable regions.

In this study, we utilize the GNSS time series provided by the NGL to train the ChangePointCNN-GNSS model. The training data set comprises daily displacement time series from approximately 2,000 stations. The displacement time series are referenced to the International GNSS Service (IGS) reference frames. The trained model is then applied to estimate site velocities at approximately 15,000 stations by identifying the longest change-point-free segment in each station's time series for each directional component (NS, north-south; EW, east-west; and UD, upper-down).

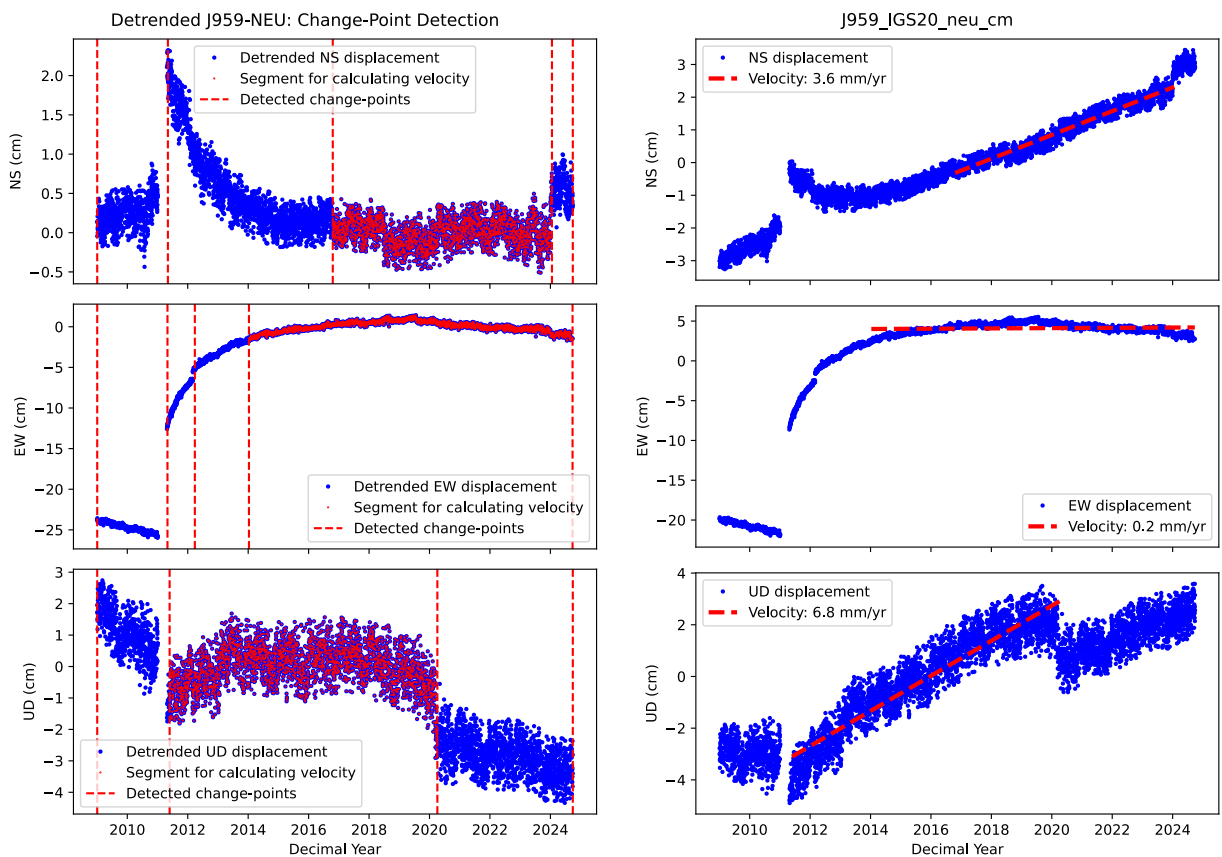


Figure 1. GNSS-derived daily displacement time series (referred to IGS20) plots at station J959 (Japan), illustrating instant and transitional change points. Instant change points bound abrupt displacements (e.g., coseismic offsets), while transitional change points define gradual displacements (e.g., postseismic deformation). The longest change-point-free segment (minimum 4 years, highlighted in red) is used for linear regression to estimate site velocity, capturing the secular crustal motion trend in this region.

2.2. Analytical Methods for Detecting Change Points

Displacement time series derived from GNSS often exhibit two distinct classes of anomalies: abrupt displacements (referred to as steps) bounded by instant change points and gradual displacements bounded by transitional change points, reflecting divergent geophysical or anthropogenic origins. Instant change points mark the start and end of abrupt displacements, characterized by near-instantaneous positional offsets, typically arising from discrete events such as equipment changes (e.g., antenna or receiver replacements, antenna mount adjustments), coseismic displacements, or sudden environmental perturbations. These change points are identified by sharp, discontinuous deviations exceeding background noise within a short period, often at a single sampling interval.

Transitional change points, in contrast, define the boundaries of gradual, nonlinear displacements evolving over weeks to years, often linked to postseismic deformation, pre- and postvolcano-eruption surface deformation, tectonic transient, slow-slip events, or anthropogenic processes, such as groundwater withdrawal-induced land subsidence. Prolonged drought events can also induce gradual displacements in GNSS time series, particularly in the vertical component, as shown by Welch et al. (2024). These displacements often follow logarithmic or exponential decay patterns, necessitating specialized detection techniques to distinguish them from secular tectonic trends. Figure 1 illustrates instant and transitional change points observed at a representative long-term GNSS station in an earthquake-prone region, with change-point-free segments highlighted in red, used for linear regression to estimate site velocities that capture secular crustal block motions.

Two common approaches are used to detect change points in time series. The first is the sliding-window method, which uses adjustable windows to scan the data for abrupt steps. The second is the rupture method (Truong et al., 2020), which applies statistical optimization to the entire time series to robustly identify change points. The sliding-window method scans detrended data by comparing mean shifts within fixed windows, tunable via

window size and threshold parameters to detect instant change points. It often misses slow, gradual displacements that span years, limiting its effectiveness for complex GNSS time series in earthquake-prone regions. In contrast, the rupture method, implemented via the ruptures library, uses dynamic programming to minimize a cost function—typically a radial basis function (rbf) kernel—across segments, offering the potential to capture both abrupt and gradual displacements by modeling nuanced changes. Yet, its conventional form is computationally intensive, making it impractical for processing decade-long GNSS time series. The rpt.KernelCPD variant, with linear complexity penalties (e.g., L1 norm), improves efficiency but sacrifices precision, frequently producing spurious change points or overlooking gradual transitions due to its reliance on simplified kernel assumptions.

To address these challenges, we implement a two-stage analytical approach, utilizing sliding-window analysis to detect instant change points and curvature-based analysis to identify transitional change points in GNSS time series. For preprocessing, we employ a robust outlier removal method that first excludes extreme displacements exceeding a 5-m absolute threshold, then detrends the time series, and iteratively filters outliers using a 360-day rolling window with a 2.5-sigma threshold over three iterations. These parameter values were optimized through extensive empirical testing on diverse GNSS data sets to achieve a primary objective: maximizing the removal of noise and outliers while rigorously preserving the integrity of the geophysical signal. This careful balancing act significantly enhances the visibility of both abrupt and gradual change points for subsequent analysis.

Instant change-point detection is performed on the detrended time series. These change points are identified using a sliding-window method that compares mean shifts between adjacent 30-day windows. To reduce false detections caused by noise, short-term environmental variations, or overly sensitive thresholds, a minimum separation of 30 days is enforced between consecutive change points. The threshold controlling the magnitude of detected abrupt steps is iteratively selected from a predefined set of candidate values during the detection process. In our implementation for global GNSS time series processing, the threshold list used for the horizontal components is (0.15, 0.2, 0.25, 0.3, 0.4, 0.5, 0.7, 1.0, 1.4, 2.0, 10.0, 20.0), while the vertical component uses (0.5, 0.6, 0.7, 0.8, 1.0, 1.2, 1.4, 1.8, 2.5, 10.0, 20.0, 30.0). The threshold values share the same unit as the displacement time series, which is typically expressed in centimeters.

To minimize the risk of undetected change points within large data gaps biasing site velocity estimates, we systematically add change points at the start and end of all gaps exceeding 1 year, since these gaps often stem from equipment replacements or antenna mount adjustments—events that typically introduce physical steps in the time series.

Transitional change-point detection targets the longest contiguous segment (>4 years) previously identified as free of instant change points during the initial sliding-window analysis. Within this segment, we first remove the linear trend. To detect the nonlinear signatures of gradual transitions, we then apply a weighted cubic polynomial fit. This model was selected after testing various approaches, including quadratic (second-order) fitting, splines, and higher-order polynomials. A cubic polynomial effectively models the curved transitions in displacement time series, providing a better fit than a quadratic function while avoiding the overfitting risks associated with more complex models like splines or higher-order polynomials. The transitional change point corresponds to a turning point in the detrended displacement time series. This is identified by finding where the first derivative (velocity) of the fitted cubic function equals zero. A weighted least-squares approach is beneficial because the timing of a transitional change often occurs in the earlier or later portions of the time series segment, rather than near the middle. The complete algorithm is implemented in the provided Python code to facilitate replication. Figure 2 illustrates typical examples of transitional change points detected by this cubic-fitting approach.

We assess whether a cubic model provides a better fit than a linear model by comparing their mean squared errors (MSE). If the absolute value of the MSE improvement ratio—calculated as the difference between the linear and cubic MSE, divided by the linear MSE—exceeds an empirically derived threshold of 0.2, the cubic model is adopted to identify potential transitional change points. This threshold was calibrated through extensive testing on a large and diverse set of GNSS time series to effectively distinguish nonlinear motion from linear noise. It serves as an initial, lower-bound filter; candidate segments that pass this threshold are then subjected to additional criteria to confirm the presence of a statistically significant transitional change point. Turning points are then identified by solving the derivative of the cubic polynomial. The amplitude of each turning point is quantified as its deviation from a baseline, defined as the mean value of the segment. If this amplitude exceeds a predefined threshold, the turning point is marked as a transitional change point. In our iterative program, these amplitude thresholds serve as key control parameters for transitional change-point detection. For the horizontal components,

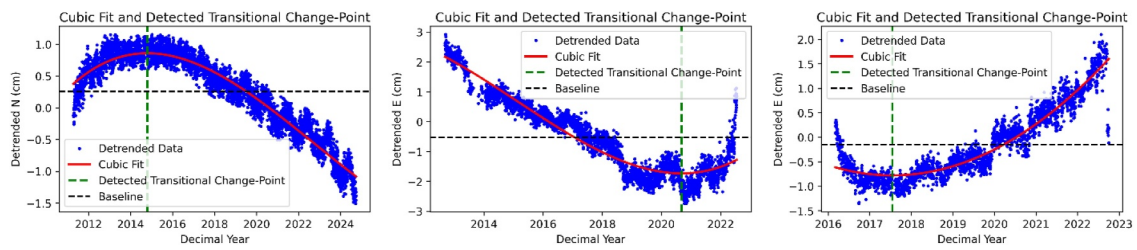


Figure 2. Detrended GNSS time series for three stations: G007 (NS component, Japan), SHUL (EW component, Taiwan), and SHWA (EW component, Taiwan), arranged from left to right. These examples illustrate the detection of transitional change points. For each plot, the longest instant-change-point-free segment, initially identified using the sliding-window method, is fitted with a cubic polynomial. The point of maximum curvature, derived from the first derivative of the cubic fit, is marked as the transitional change point.

candidate thresholds of 0.4, 0.6, and 1.0 (in data units) are used; for the vertical component, thresholds of 0.5, 0.8, and 1.2 are applied.

2.3. Estimation of Site Velocity and Its Uncertainty

Determining optimal thresholds for change point detection is a complex calibration problem, as requirements vary significantly between stations and even between components at a single site, making manual tuning impractical for large-scale data sets. To automate this process, we developed an AI-driven framework that iteratively tests each candidate configuration of thresholds from a predefined pool—established for detecting instant and, where necessary, transitional change points, as described in the previous section. For each configuration, the algorithm generates a time series plot with all detected change points clearly marked. A CNN model then evaluates the suitability of each plot for reliable velocity estimation and assigns a corresponding probability score.

The iterative process is designed for computational efficiency: if any configuration achieves a high confidence score of 0.85 or above, the iteration stops early and that configuration is selected. If no configuration meets this score, the process exhaustively tests all candidates and selects the one with the highest score. The final selected configuration is used to identify the longest change-point-free segment.

In our method, site velocities are estimated using linear regression applied to the longest change-point-free segment, provided it spans at least 4 years. This minimum 4-year duration is a critical criterion, ensuring both statistical reliability and geophysical relevance of the velocity estimates. First, the empirical analysis of three-component displacement time series from approximately 9,700 global GNSS stations demonstrates that the 95% confidence interval (95% CI) of the linear trends decreases exponentially with the duration of continuous observations (Figure 3) (Cornelison & Wang, 2023; Wang, 2022). The 95% CI is widely used as a measure of uncertainty for GNSS-derived site velocities. Typically, horizontal velocities achieve about 1 mm/year uncertainty (95% CI) with 2.5 years of uninterrupted data, while vertical velocities require about 4 years to reach the same level of uncertainty. Extending the observation length beyond 7 years further reduces uncertainties below 0.5 mm/year across all components. In general, beyond about 4 years, additional data yield only marginal reduction in velocity uncertainty, suggesting a practical limit to accuracy gains. Based on this, we impose a minimum 4-year threshold for change-point-free segments, ensuring a 95% CI of below 1 mm/year for the estimated site velocity. This precision threshold is a commonly adopted standard in geodetic studies for resolving secular tectonic signals and longer-term deformation processes.

Second, step correction is deliberately avoided in large-scale analyses. Equipment-related abrupt steps (e.g., antenna changes) are often accounted for during the processing calculating daily positions from GNSS raw data, Receiver Independent Exchange Format (RINEX) files, if these changes are recorded in the site log of the station. However, undocumented equipment changes or environmental perturbations can cause complex steps in GNSS time series. Correcting these steps manually for individual time series, though feasible in certain cases (e.g., Wang, 2023; Wang et al., 2022), could introduce subjective errors that amplify velocity uncertainties. More critically, automated step correction across vast GNSS data sets is computationally prohibitive and error-prone due to station-specific variability in steps and noise characteristics. By favoring change-point-free segments over step-corrected data, our framework avoids these challenges while still achieving reliable velocity estimates.

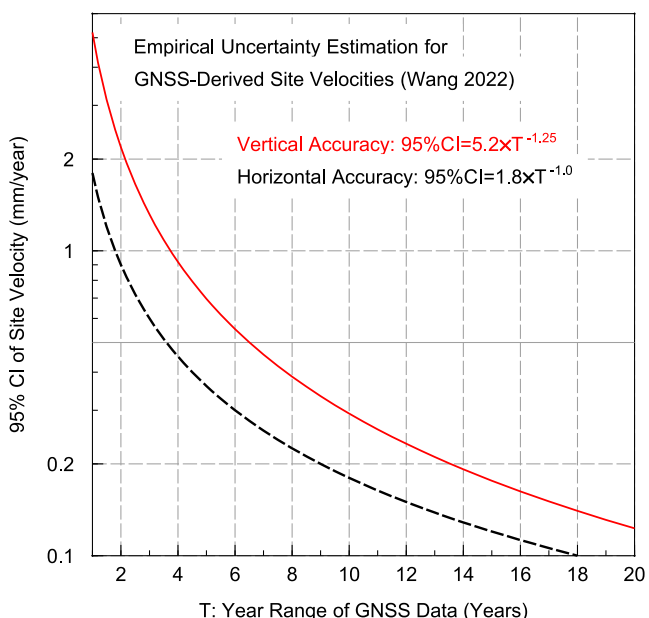


Figure 3. Curves illustrating empirical formulas that model the 95% confidence interval (95% CI) for horizontal and vertical site velocities derived from GNSS daily displacement time series. The empirical formulas used to generate these curves are adapted from Wang (2022).

sible interface for transfer learning in deep learning applications. Renowned for its powerful performance in image recognition tasks, VGG16 excels at identifying subtle visual patterns, making it an ideal foundation for our change-point-detection assessment model via transfer learning. This approach leverages VGG16's robust feature extraction capabilities, minimizing the computational resources and training data needed for high accuracy.

We adopted a two-phase training strategy to optimize performance for binary classification of GNSS change-point-detection plots (“good” vs. “bad”). In Phase 1, we froze the VGG16 convolutional base and appended custom dense layers: a flatten layer to linearize the convolutional output, followed by two fully connected layers (256 and 128 neurons, ReLU activation) with dropout rates of 0.5 and 0.3, respectively, to mitigate overfitting, and a final sigmoid output layer for binary classification. This phase, compiled with the Adam optimizer (learning rate 10^{-4}) and binary cross-entropy loss, trained the top layers for 10 epochs. An epoch refers to one complete pass through the entire training data set during the learning process. In Phase 2, we unfroze the top eight VGG16 layers for fine-tuning, recompiling with a lower learning rate (2×10^{-5}) and training for up to 30 epochs, using early stopping (patience of 5) to prevent overfitting and retain the best validation accuracy.

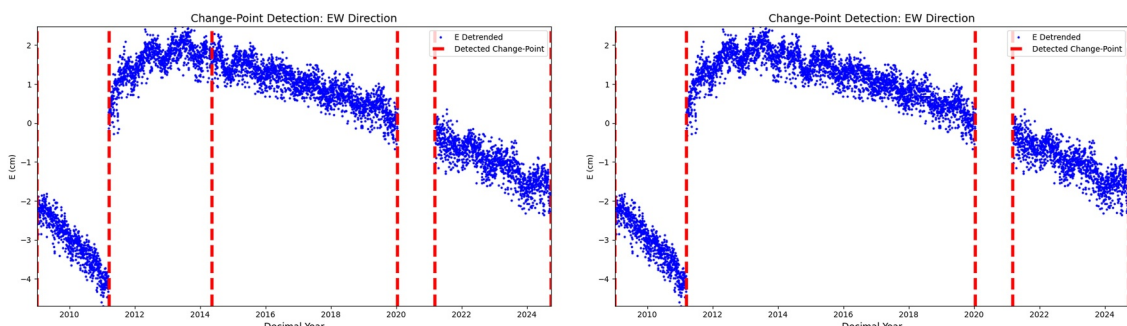


Figure 4. Sample training plots of detrended east-west (EW) displacement time series for station G009 in Japan, illustrating examples used to train the CNN model: ChangePointCNN-GNSS. Each plot shows detected change points along with markers at the beginning and end of a large data gap (>1 year). The left image is labeled “good”, as it correctly identifies both instant and transitional change points, making it suitable for reliable site velocity estimation. The right image is labeled “bad”, as it fails to detect the transitional change point, making the configuration unsuitable for site velocity estimation.

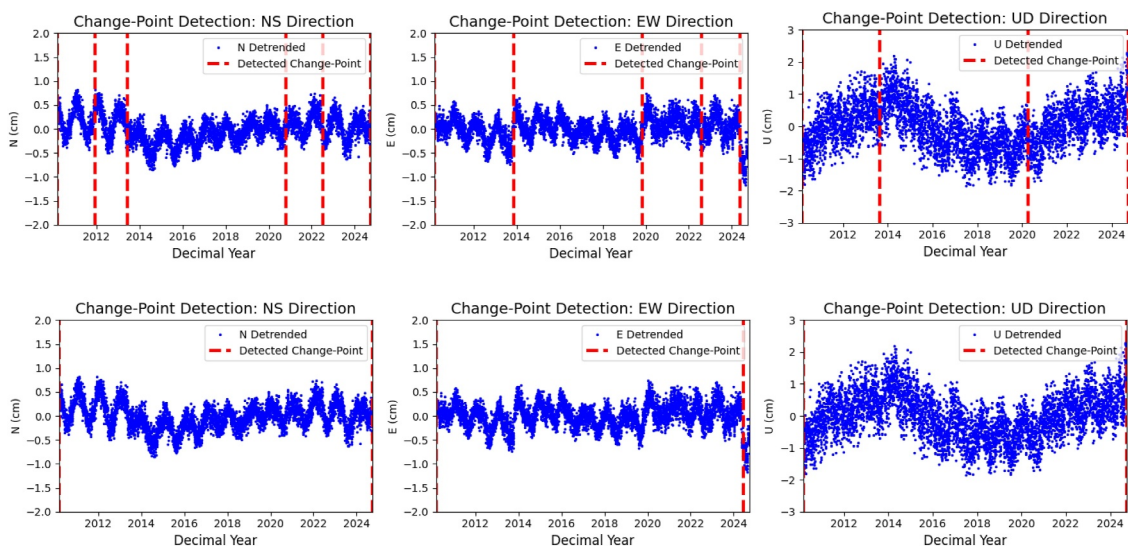


Figure 5. Three-component (NS, EW, UD) detrended displacement time series for GNSS station TXDL in Dalhart, northern Texas, showing seasonal horizontal motions (NS, EW) and decade-scale sinusoidal vertical fluctuations (UD) possibly tied to groundwater cycles. First-row subplots display change points identified using a sliding-window method (instant change points, NS and EW components) and a cubic-fitting method (transitional change points, UD component), purposefully labeled as “bad” for CNN training. Second-row subplots exclude these change points associated with minor displacements and are labeled as “good” for CNN training.

Training plots were standardized to 224×224 pixels, and random horizontal flips were applied during data augmentation using TensorFlow’s `ImageDataGenerator` (Abadi et al., 2016). Horizontal flips mirror the time series plots across the vertical axis, effectively simulating a reversal of the time direction (e.g., from left-to-right to right-to-left), which ensures the model learns to detect displacement patterns regardless of the temporal orientation of the GNSS data. The resulting model is saved as `ChangePointCNN-GNSS.keras`. For a detailed understanding of the training methodology, readers are encouraged to refer to the Python program, `Train_ChangePointCNN-GNSS.py`.

To determine the optimal pretrained model for our `ChangePointCNN-GNSS` architecture, we also evaluated ResNet50 as a feature extractor for classifying GNSS change-point detection plots. ResNet50 is a 50-layer CNN with residual connections (He et al., 2016). It excels in deep learning tasks by mitigating vanishing gradient issues, making it a robust feature extractor for image-based classification. Its pretrained weights support transfer learning for specialized applications like our GNSS time series plot analysis.

Both models were trained in two phases: initial training with frozen base layers and fine-tuning of the top layers. VGG16 achieved a peak validation accuracy of 0.90 and a minimum validation loss of 0.45, slightly outperforming ResNet50, which reached 0.82 validation accuracy and a minimum validation loss of 0.63. Despite ResNet50’s deeper architecture, its performance was hindered by overfitting, as evidenced by a higher final validation loss (0.63 vs. VGG16’s 0.45), likely due to its complexity relative to our moderate data set size. VGG16’s simpler architecture provided better generalization and stability for our task, leading to its selection as the pretrained model for the `ChangePointCNN-GNSS` pipeline.

3.3. Educating the CNN for Omitting Minor Instant and Transitional Displacements

Traditional change-point detection, particularly for transitional change points, faces inherent limitations: the criteria for identifying change points vary significantly across research objectives and spatiotemporal scales, complicating the establishment of universal rules. Even among experts, subjective interpretations often yield inconsistent change-point identification, particularly when distinguishing between physical displacements and nonphysical signals.

For long-term site velocity estimation, we prioritize omitting minor instant and transitional displacements to secure longer change-point-free segments. To train the model with this objective in mind, we labeled numerous plots containing detected change points associated with minor displacements as “bad” and those omitting these

change points as “good.” Figure 5 showcases several examples of these labeled plots, illustrating the omission of change points associated with minor displacements in change-point detection.

Minor displacements in GNSS time series often arise from nontectonic influences such as transient noise, multipath effects, or localized environmental factors (e.g., short-term droughts, vegetation changes, fluctuations of groundwater levels). These artifacts manifest spurious displacements—sometimes as alternating positive and negative instant or transitional displacements. Over multiyear timescales, such random fluctuations tend to cancel out, leaving the long-term linear trend largely unaffected. Including change points associated with these minor displacements may lead to overfitting of noise or misinterpretation of short-term variations as long-term deformation trend, particularly in vertical displacement analyses where seasonal and environmental signals are prominent. By omitting change points associated with minor displacements, we prioritize segments of uninterrupted motion that robustly capture the site’s secular velocity. However, the determination of which change points to exclude or include is somehow subjective, guided by research objectives and experience (see Figure 5).

Our AI-driven approach resolves this ambiguity by training the CNN on meticulously curated data sets, enabling it to implicitly learn context-dependent distinctions from expert-labeled examples. This ensures methodological consistency while retaining adaptability to varied geophysical contexts. Through repeated exposure to nuanced cases, the model autonomously determines optimal change-point configurations tailored to specific objective, accurately estimating long-term site velocities. By doing so, the CNN-guided framework outperforms rigid rule-based methods, demonstrating flexibility in handling the complexities of GNSS data analysis. This hybrid approach facilitates reliable velocity estimates across diverse tectonic, anthropogenic, and environmental settings.

3.4. Model Accuracy and Probability Score

The ChangePointCNN-GNSS model is designed to assess the suitability of analytically detected change points for reliable site velocity estimation from GNSS time series. The training data set is split into 80% for training and 20% for validation. In addition, we created an independent test set comprising approximately 10% of the training data set size, which were not used during training or validation. These test images were carefully selected to include a representative balance of both “good” and “bad” cases, ensuring a robust and unbiased evaluation of the model’s performance.

In the CNN training program, validation and test data sets serve distinct roles. The validation data set guides model training by monitoring the generalization capability of the model, tuning hyperparameters (such as learning rate and batch size), and detecting convergence or potential overfitting. In contrast, the test data set is evaluated only after training concludes, providing an unbiased estimate of the model’s performance on completely independent data. The CNN model achieved a validation accuracy of 0.90 and a test accuracy of 0.89. Considering the inherent ambiguity in labeling training images strictly as “good” or “bad”—since many change-point plots are subjectively rated as “OK,” meaning neither distinctly good nor clearly bad, and thus inconsistently labeled—the achieved accuracy values near 0.9 are notably high.

Rather than providing a binary classification of “good” or “bad,” the CNN model outputs a probability score ranging from 0 to 1 as an assessing result for each input image. The probability score is defined as the model’s predicted probability that a plot belongs to the “good” class using a sigmoid activation function. This probabilistic approach, leveraging the sigmoid activation in the final dense layer, allows for nuanced assessment, enabling the model to rank candidate change-point configurations based on their likelihood of being optimal. This scoring mechanism is critical for our application, as it facilitates the selection of the most appropriate change-point configuration for each GNSS time series. The average probability score for “good” images in the test data sets is 0.87 and the average score for “bad” images is 0.1. These scores demonstrate the model’s effectiveness by showing a clear distinction between suitable (good) and unsuitable (bad) plots, underscoring its ability to accurately differentiate between the two.

In practical applications, the CNN model evaluates multiple candidate change-point-detection plots for each time series, with each plot generated using a different configuration of analytical parameters. These plots, derived from the sliding-window and cubic-fitting methods, are scored by the CNN. The iterative process selects the first parameter configuration that meets or exceeds a probability score threshold of 0.85; if none are found, the configuration with the highest score after evaluating all candidates is selected. This ensures the identification of

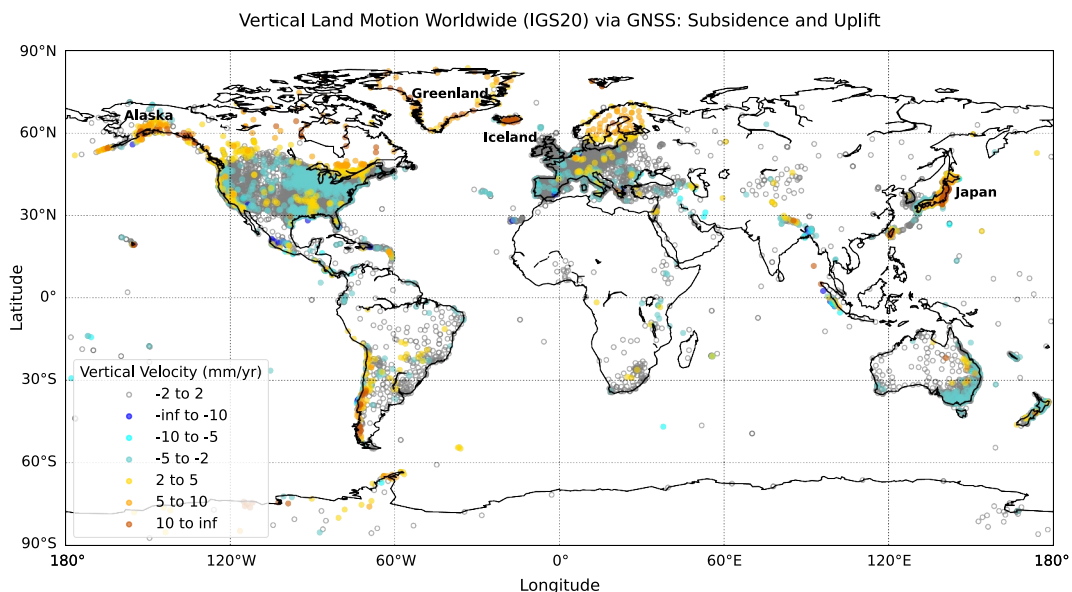


Figure 6. Map illustrating global vertical land motion patterns derived from GNSS data (~12,500 stations). Vertical velocities (IGS20) are shown in millimeters per year (mm/year) using a color-coded scale.

optimal parameter settings, which enhances the precision of site velocity estimates by reliably identifying the longest change-point-free segment for linear regression.

4. Results

The methods introduced in this study are integrated into a Python program, *GNSS_CPD_VelocityEstimation.py*, which efficiently computes site velocities for approximately 15,000 GNSS sites in about 2 days on a Dell Precision workstation equipped with the Intel® Xeon® W3-2423 processor (6 cores, up to 4.2 GHz) and 64 GB of RAM. The station information and estimated site velocities (IGS20) are provided in the data set archived on Zenodo (Wang et al., 2025; file: IGS20_Velocities_at_Global_GNSS.txt).

Figure 6 illustrates the long-term vertical ground motion velocities at approximately 12,500 global GNSS sites, providing a global perspective on land uplift and subsidence patterns. The site velocities are aligned to the International GNSS Service 2020 (IGS20) reference frame (Reischburg et al., 2022). While velocities were calculated for approximately 15,000 stations, we omitted those with extreme vertical velocities and consolidated collocated or closely spaced stations to a single representative site to enhance map readability and avoid visual clutter. The map reveals that land uplift follows distinct and widespread patterns across the globe, with yellow to orange dots indicating uplift rates of 2 to over 10 mm/year, while subsidence, marked by cyan to blue dots, appears less prevalent on a global scale. Many uplift patterns align with well-established glacial isostatic adjustment (GIA) processes, as documented in regions like Scandinavia (notably Sweden and Finland), Greenland, Iceland, and much of Canada (e.g., Caron et al., 2018; Peltier et al., 2015; Zhou et al., 2020), where the Earth's crust continues to rebound following the retreat of glaciers from the last Ice Age, often at rates around a few mm/year.

The most significant uplift patterns are driven by tectonic activity, particularly in tectonically active zones such as the eastern coastal region of Japan, central Taiwan, the Alaskan coast extending to the western coast of the United States, and the western coast at the southern tip of South America, where active plate interactions generate substantial uplift, frequently surpassing 5 mm/year. These subsidence and uplift patterns, consistent with previous global vertical land movement studies (e.g., Hammond et al., 2021), demonstrate the ChangePointCNN-GNSS model's ability to refine site velocity estimates, providing insights into geodynamic processes, regional tectonics, and sea-level changes.

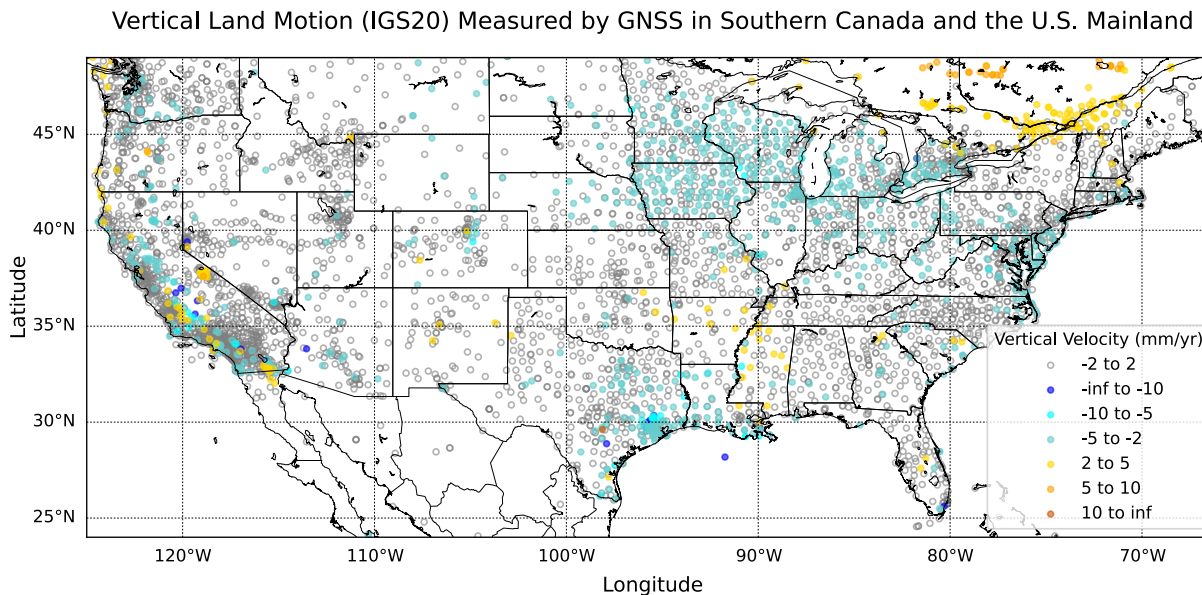


Figure 7. Map showing the magnitude of vertical land motion derived from GNSS data across southern Canada and the contiguous United States. Vertical velocities (IGS20) are shown in millimeters per year (mm/year) using a color-coded scale.

A detailed analysis of Figure 7, which zooms into southern Canada and the U.S. mainland, highlights a distinct uplift pattern in the middle-south U.S. along the Mississippi River, where yellow dots indicate uplift rates of 2–5 mm/year. This uplift is particularly striking because the region, encompassing eastern Texas, Arkansas, western Tennessee, and Mississippi, is generally regarded as an area experiencing minor land subsidence due to groundwater extraction (e.g., Galloway et al., 1999; Rodgers & Whaling, 2020; Traylor et al., 2024; Turco et al., 2025). The observed uplift may be attributed to understudied processes such as isostatic responses to sediment unloading, subtle tectonic adjustments, groundwater storage recovery in large aquifer systems (Larochelle et al., 2022), though these mechanisms remain poorly documented in this area. Additionally, Figure 7 also reveals pronounced subsidence around the Great Lakes region, including Michigan, Wisconsin, Minnesota, northern Illinois, northern Indiana, and southern Ontario, Canada, with subsidence rates often ranging from 2 to 5 mm/year, likely driven by a combination of GIA relaxation (e.g., Kreemer et al., 2018), groundwater withdrawal for agricultural irrigation, and rise of Great Lakes surface water (Argus et al., 2020).

These contrasting patterns, uncovered through the large-scale application of our automated method, highlight the significance of high-accuracy, globally consistent site velocities. The efficiency and reliability of our approach provide a new tool for the research community to identify previously overlooked regions of land motion and explore their underlying causes and implications for global and regional-scale sea-level change and tectonic studies.

5. Discussion

5.1. Comparison With MIDAS Velocities

Our global process identified approximately 14,600 GNSS stations with at least 4-year-long change-point-free segments in all three components (NS, EW, UD). For a follow-up review, we compared velocities derived from our method with those from MIDAS for these stations. This comparison serves as a diagnostic tool rather than a validation of our velocities, as MIDAS does not provide a definitive ground truth for secular velocities in complex GNSS data sets (Blewitt et al., 2016). At about 12,200 stations (approximately 90% of the data set), the velocity differences are less than 2 mm/year in all directions, indicating strong agreement between the two methods despite their differing approaches.

In contrast to our segment-based approach, which isolates a single longest stable segment, MIDAS derives a velocity by calculating the median rate from the slopes of all possible 1-year data pairs within the entire time

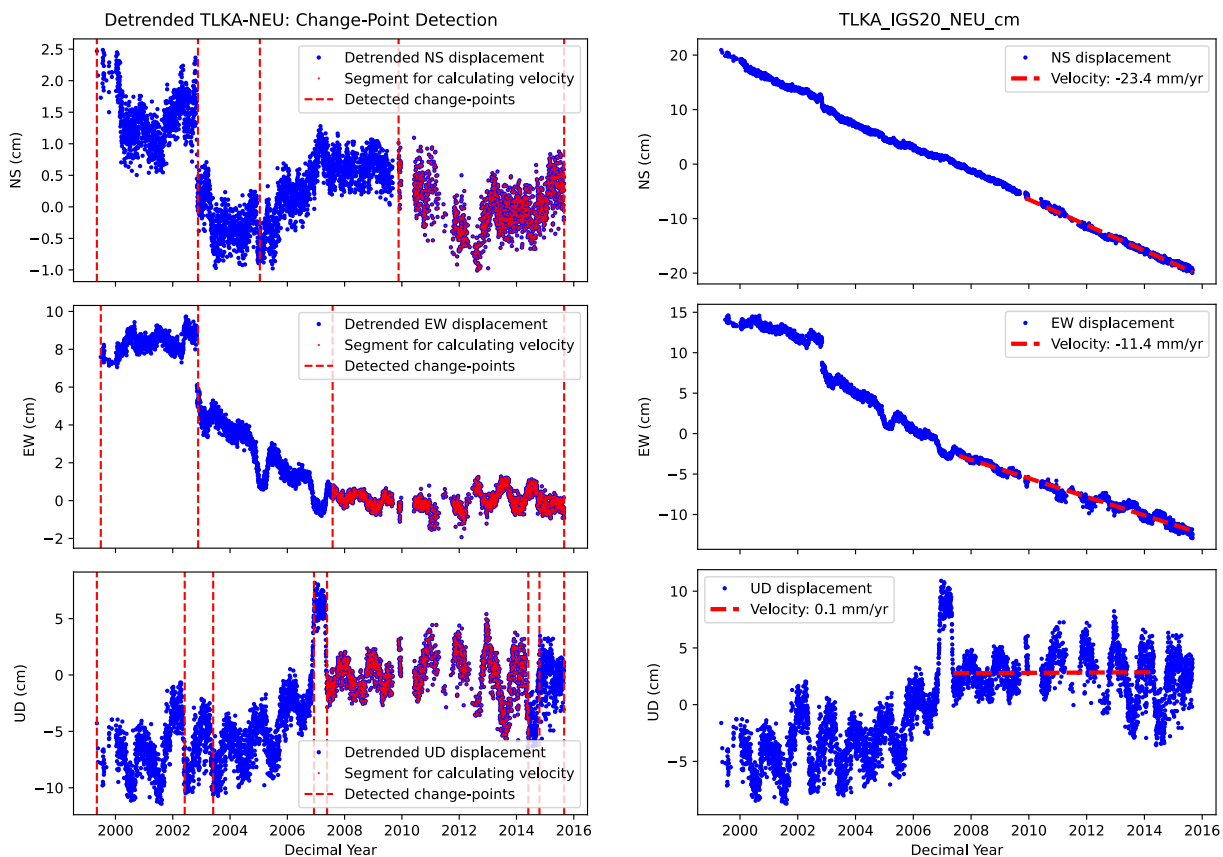


Figure 8. Change-point detection and site velocity estimates for GNSS station TLKA, located ~115 km north of Anchorage, Alaska. (Left panel) Detrended daily displacement time series (2000–2015) with detected instant and transitional change points; the longest change-point-free segment in each time series, used for site velocity estimation, is highlighted in red. (Right panel) Displacement time series (relative to IGS20) with estimated site velocities. A prominent step in the horizontal components reflects coseismic displacement from the 2002 Denali earthquake (M 7.9, 3 November 2002).

series, without explicit change-point detection (Blewitt et al., 2016). This method effectively resists outliers by using the median statistic, while our method prioritizes the identification of a single, long-term stable segment to ensure low velocity uncertainties. The key difference lies in their handling of nonlinear motion; a significant discrepancy (e.g., >2 mm/yr) between their estimated velocities serves as a robust indicator that a station's time series likely contains complex deformation signals or undocumented disturbances. Therefore, for global or regional analyses, we recommend cross-verifying velocities from both methods, as provided in the comparative data set archived on Zenodo (Wang et al., 2025; file: IGS20_Velocities_CNN_MIDAS.txt). Stations where differences exceed 2 mm/year are prime candidates for expert, case-by-case analysis, requiring a manual review of the time series plots to determine the most appropriate velocity, as no single method can guarantee optimal estimates for all applications given the complex nature of real ground motions and GNSS noise patterns.

5.2. Linking Secular and Site Velocities

Secular velocities in geodesy and tectonics refer to the long-term, steady rates of tectonic plate motion, averaging out transient effects like seasonal variations or earthquake-induced displacements. These velocities represent the consistent background movement of the Earth's crust over extended periods. In contrast to idealized secular velocities, our site velocity estimates may reflect station-specific temporal complexities. By integrating the ChangePointCNN-GNSS model with analytical techniques, our approach delivers robust velocity estimates that align closely with secular velocities in tectonically stable regions. In regions with frequent earthquakes or volcanic activity, site velocities primarily reflect secular motion but may be partially biased by ongoing postseismic

deformation or long-term volcanic processes, which can continue for years to decades. Researchers must account for these differences when using the site velocity to interpret crustal deformation and assessing hazards in such regions.

Figure 8 presents the three-component displacement time series (relative to IGS20) for the TLKA GNSS station, highlighting detected change points. The TLKA station is located in Alaska in south-central, approximately 115 km north of Anchorage. The station lies in a tectonically active region influenced by the interaction of the Pacific and North American plates and numerous active faults. The left panel shows instant and transitional change points, while the right panel identifies the longest change-point-free segments used for site velocity estimation. A significant step in the horizontal components reflects coseismic displacements from the 2002 Denali earthquake (M 7.9, 3 November 2002). This station is located approximately 200 km from the epicenters of the 2002 Denali and the 1964 Alaska (M 9.2, 27 March 1964) earthquakes. Postseismic deformation from the 2002 Denali earthquake was significant for about 5 years as depicted in the displacement time series, and postseismic displacements (residual effect) from the 1964 earthquake may still contribute to present-day crustal displacements in the TLKA area (e.g., Suito & Freymueller, 2009).

Thus, deriving precise secular velocities for the tectonic block in this region is challenging due to these effects. Our method effectively identifies stable segments for estimating site velocities, minimizing disruptions from the 2002 Denali earthquake. The resulting velocities provide the best estimates of long-term tectonic block motion in this area. The MIDAS method estimates velocities at TLKA as -22.1 (NS), -15.4 (EW), and 11.7 (UD) mm/year. In contrast, our method yields velocities of -23.4 (NS), -11.4 (EW), and 0.1 (UD) mm/year. The horizontal velocity differences between the two methods are in the order of a few mm/year, while the vertical velocity difference reaches up to 10 mm/year. Our velocity estimates minimize the potential impact of postseismic displacements by omitting approximately 6 years of data (with slightly different durations for each of the three components) following the Denali earthquake.

For studies in complex tectonic settings, we recommend inspecting time series plots on a case-by-case basis to select the most appropriate velocity for specific research objectives, as the choice of velocity depends on the study's objectives, such as interseismic and long-term crustal motion studies and landslide monitoring (e.g., Wang et al., 2015).

5.3. Machine Learning: From Data-Driven Models to Image-Driven Assessment

Under the broad umbrella term of AI, machine learning (ML) is a specialized domain where algorithms are designed to learn from data and subsequently make predictions or informed decisions. Within ML, an advanced subset known as deep learning (DL) employs neural networks composed of multiple layers to address complex tasks, such as image recognition and speech processing. A further specialized category within DL, known as CNNs, excels specifically at analyzing spatial patterns in images, such as those representing change-point configurations in GNSS time series plots. Unlike conventional ML techniques that rely heavily on manually engineered statistical or sequential features extracted from time series, the CNN method adopted in this study directly learns temporal patterns from visual representations of displacement time series and change-point plots, closely emulating the visual reasoning and context-awareness of human experts.

A wide variety of ML approaches, including random forest, multilayer perceptron (MLP), extreme gradient boosting (XGBoost), linear support vector classification (LSVC), and long short-term memory (LSTM) methods, have previously been applied to GNSS time series analysis (e.g., Chen et al., 2023; Crocetti et al., 2021; Gao et al., 2022; Li et al., 2023; Özbey et al., 2024; Wang et al., 2021; Xie et al., 2023). These data-driven methods typically utilize predefined statistical features or temporal assumptions to detect anomalies or discontinuities. Commonly used features include statistical metrics (e.g., mean, standard deviation, skewness, kurtosis), frequency-domain characteristics (Fourier coefficients), trend indicators (linear or polynomial regression coefficients), and displacement metrics (e.g., maximum, minimum, range, step-detection thresholds). However, reliance on these manually crafted features can limit the flexibility and adaptability of these methods, particularly when dealing with context-specific change-point detection scenarios across diverse GNSS stations exhibiting varied noise levels, data gaps, and geophysical signals. Moreover, these traditional ML techniques often require extensive feature engineering or detailed labeling of training data.

Recently, one-dimensional CNNs (1D CNNs) have demonstrated exceptional performance across various applications involving time series data (e.g., Ismail Fawaz et al., 2019; Kiranyaz et al., 2021), including biomedical signal classification (Kiranyaz et al., 2017) and structural health monitoring (Abdeljaber et al., 2017). 1D CNN is a data-driven method, which processes sequential data using convolutional filters to capture temporal patterns. By directly processing sequential displacement data, 1D CNNs could detect subtle trends and anomalies relevant to tectonic and nontectonic signals within GNSS data. Future research might explore hybrid models integrating 1D CNNs with analytical approaches to further enhance robustness, computational efficiency, and interpretability in complex GNSS data sets.

In contrast to purely data-driven AI methods, this study introduces a hybrid analytical-CNN framework that integrates physical modeling with image-based evaluation. Specifically, we adopt a two-dimensional convolutional neural network (2D CNN), a model designed to process spatial patterns and features in visual representations, typically images. Leveraging transfer learning from a large pretrained CNN, our 2D CNN analyzes synthetic “scenes”—visual plots of displacement time series annotated with analytically detected change points. By evaluating these visual representations holistically, the 2D CNN performs a task analogous to expert visual judgment, identifying and prioritizing change-point-free segments to optimize site-velocity estimation.

Our decision to represent GNSS time series and candidate change points as images, subsequently evaluated by a 2D CNN, is strategically motivated by our primary objective of accurately estimating long-term site velocities. This estimation depends on selecting a suitable overall configuration of change points rather than focusing on the identification of individual change points from raw data. This image-based approach offers several advantages.

1. It closely mimics the visual inspection performed by geodetic experts, capturing contextual nuances—such as the alignment of change points with geophysical events or data gaps—while disregarding minor displacements that are challenging to encode numerically.
2. It simplifies training data annotation, requiring only binary classifications (“good” or “bad”), thus eliminating the need for granular labeling (exact change-point positions) required by data-drive ML methods.
3. By leveraging transfer learning from pretrained CNN models, it achieves high validation accuracy with relatively modest training data sets, promoting scalability across diverse GNSS networks.
4. It integrates seamlessly with the hybrid analytical framework (sliding-window and cubic-fitting techniques), enabling efficient ranking of candidate configurations according to their suitability for precise long-term site velocity estimation.

6. Conclusions

This study significantly advances the field of geodesy through two key contributions: the development of the AI model ChangePointCNN-GNSS.keras and the generation of reliable site velocities (IGS20) for approximately 14,600 GNSS stations worldwide. To promote transparency and reproducibility, we have publicly released all supporting materials, including the training and test data sets, the training script (Train_ChangePointCNN-GNSS.py), and the integrated processing tool (GNSS_CPD_VelocityEstimation.py) (Wang et al., 2025). These open-source tools are designed to be easily adapted for different GNSS data sets or customized research goals. Beyond GNSS, the methodological framework is applicable to other geophysical time series such as those from tide gauges, extensometers, groundwater wells, and meteorological stations, enabling broad interdisciplinary use. Ultimately, this study lays the foundation for robust, image-driven AI methodologies for large-scale geophysical monitoring worldwide.

Conflict of Interest

The authors declare no conflicts of interest relevant to this study.

Data Availability Statement

The raw GNSS time series were obtained from the Nevada Geodetic Laboratory (<https://geodesy.unr.edu>). The complete set of derived materials for this study has been permanently archived on Zenodo (Wang et al., 2025). This archive includes the training data set, Python source code (for both model training and application), the pretrained CNN model, and the final catalog of IGS20 site velocities for approximately 14,600 stations. All files

are accessible through the DOI: <https://doi.org/10.5281/zenodo.17180354>. The project's development history can be viewed on the first author's GitHub page (<https://github.com/bob-Github-2020>).

Acknowledgments

This research would not have been feasible without the global GNSS displacement time series provided by the Nevada Geodetic Laboratory (NGL). The authors express their gratitude to Drs. Geoffrey Blewitt, Corné Kreemer, and Bill Hammond for their invaluable contribution in making these high-quality GNSS data sets openly accessible, enabling advancements in geodetic research. The authors sincerely appreciate the editors and the four anonymous reviewers for their invaluable time and constructive comments on our manuscript. Their insightful critiques and thoughtful suggestions have been instrumental in significantly improving the clarity, depth, and overall quality of this paper.

References

- Abadi, M., Agarwal, A., Barham, P., Brevdo, E., Chen, Z., Citro, C., et al. (2016). TensorFlow: Large-scale machine learning on heterogeneous systems. *arXiv:1603.04467* <https://arxiv.org/abs/1603.04467>
- Abdeljaber, O., Avci, O., Kiranyaz, S., Gabbour, M., & Inman, D. J. (2017). Real-time vibration-based structural damage detection using one-dimensional convolutional neural networks. *Journal of Sound and Vibration*, 388, 154–170. <https://doi.org/10.1016/j.jsv.2016.10.043>
- Agudelo, G., Wang, G., Liu, Y., Bao, Y., & Turco, M. J. (2020). GPS geodetic infrastructure for subsidence and fault monitoring in Houston, Texas, USA. *Proceedings of IAHS*, 382, 11–18. <https://doi.org/10.5194/piahs-382-11-2020>
- Altamimi, Z., Rebischung, P., Collilieux, X., Métivier, L., & Chanard, K. (2023). ITRF2020: An augmented reference frame refining the modeling of nonlinear station motions. *Journal of Geodynamics*, 97(47), 47. <https://doi.org/10.1007/s00190-023-01738-w>
- Argus, D. F., Peltier, W. R., Drummond, R., Borsa, A. A., Wiese, D. N., Blewitt, G., et al. (2020). Rise of Great Lakes surface water, sinking of the upper Midwest of the United States, and viscous collapse of the forebulge of the former Laurentide ice sheet. *Journal of Geophysical Research: Solid Earth*, 125(9), e2020JB019739. <https://doi.org/10.1029/2020JB019739>
- Bao, Y., Yu, X., Wang, G., Zhou, H., Ding, X., Xiao, G., et al. (2021). SCIna20: A stable geodetic reference frame for ground movement and structural deformation monitoring in South China. *Journal of Surveying Engineering*, 147(3), 04021006. [https://doi.org/10.1061/\(ASCE\)SU.1943-5428.0000352](https://doi.org/10.1061/(ASCE)SU.1943-5428.0000352)
- Bedford, J., & Bevis, M. (2018). Greedy automatic signal decomposition and its application to daily GPS time series. *Journal of Geophysical Research: Solid Earth*, 123(8), 6992–7003. <https://doi.org/10.1029/2017jb014765>
- Bevis, M., & Brown, A. (2014). Trajectory models and reference frames for crustal motion geodesy. *Journal of Geodesy*, 88(3), 283–311. <https://doi.org/10.1007/s00190-013-0685-5>
- Blewitt, G., Hammond, W. C., & Kreemer, C. (2018). Harnessing the GPS data explosion for interdisciplinary science. *Eos*, 99(10), 485. <https://doi.org/10.1029/2018EO104623>
- Blewitt, G., Kreemer, C., Hammond, W., & Goldfarb, J. M. (2013). Terrestrial reference frame NA12 for crustal deformation studies in North America. *Journal of Geodynamics*, 72, 11–24. <https://doi.org/10.1016/j.jog.2013.08.004>
- Blewitt, G., Kreemer, C., Hammond, W. C., & Gazeaux, J. (2016). MIDAS robust trend estimator for accurate GPS station velocities without step detection. *Journal of Geophysical Research: Solid Earth*, 121(3), 2054–2068. <https://doi.org/10.1002/2015JB012552>
- Caron, L., Ivins, E. R., Larour, E., Adhikari, S., Nilsson, J., & Blewitt, G. (2018). Gia model statistics for grace hydrology, cryosphere, and ocean science. *Geophysical Research Letters*, 45(5), 2203–2212. <https://doi.org/10.1002/2017GL076644>
- Chen, H., Lu, T., Huang, J., He, X., Yu, K., Sun, X., et al. (2023). An improved VMD-LSTM model for time-varying GNSS time series prediction with temporally correlated noise. *Remote Sensing*, 2023, 15(14), 3694. <https://doi.org/10.3390/rs15143694>
- Cornelison, B., & Wang, G. (2023). GNSS_Vel_95CI.py: A python module for calculating the uncertainty of GNSS-derived site velocity. *Journal of Surveying Engineering*, 149(1), 06022001. [https://doi.org/10.1061/\(ASCE\)SU.1943-5428.0000410](https://doi.org/10.1061/(ASCE)SU.1943-5428.0000410)
- Crocetti, L., Schartner, M., & Soja, B. (2021). Discontinuity detection in GNSS station coordinate time series using machine learning. *Remote Sensing*, 13(19), 3906. <https://doi.org/10.3390/rs13193906>
- Deng, J., Dong, W., Socher, R., Li, L. J., Li, K., & Li, F. F. (2009). ImageNet: A large-scale hierarchical image database. In *2009 IEEE Conference on computer vision and pattern recognition* (pp. 248–255). <https://doi.org/10.1109/CVPR.2009.5206848>
- Galloway, D. L., Jones, D. R., & Ingebritsen, S. E. (1999). *Land subsidence in the United States* (Vol. 1182). U.S. Geological Survey Circular. Retrieved from <https://pubs.usgs.gov/circ/circ1182/>
- Gao, W., Li, Z., Chen, Q., Jiang, W., & Feng, Y. (2022). Modelling and prediction of GNSS time series using GBDT, LSTM and SVM machine learning approaches. *Journal of Geodesy*, 96(10), 71. <https://doi.org/10.1007/s00190-022-01662-5>
- Gazeaux, J., Williams, S., King, M., Bos, M., Dach, R., Deo, M., et al. (2013). Detection of offsets in GPS experiment. *Journal of Geophysical Research: Solid Earth*, 118(5), 2397–2407. <https://doi.org/10.1002/jgrb.50152>
- Griffiths, J., & Ray, J. (2016). Impacts of GNSS position offsets on global frame stability. *Geophysical Journal International*, 204(1), 480–487. <https://doi.org/10.1093/gji/ggv455>
- Hammond, W. C., Blewitt, G., Kreemer, C., & Nerem, R. S. (2021). Global vertical land motion for studies of sea level rise. *Journal of Geophysical Research: Solid Earth*, 126(7), e2021JB022355. <https://doi.org/10.1029/2021jb022355>
- He, K., Zhang, X., Ren, S., & Sun, J. (2016). Deep residual learning for image recognition. In *Proceedings of the IEEE Conference on computer vision and pattern recognition* (pp. 770–778). <https://doi.org/10.48550/arXiv.1512.03385>
- Heflin, M., Donnellan, A., Parker, J., Lyzenga, G., Moore, A., Ludwig, L. G., et al. (2020). Automated estimation and tools to extract positions, velocities, breaks, and seasonal terms from daily GNSS measurements: Illuminating nonlinear Salton trough deformation. *Earth and Space Science*, 7(7), e2019EA000644. <https://doi.org/10.1029/2019EA000644>
- Herring, T. A., Melbourne, T. I., Murray, M. H., Floyd, M. A., Szeliga, W. M., King, R. W., et al. (2016). Plate boundary observatory and related networks: GPS data analysis methods and geodetic products. *Reviews of Geophysics*, 54(4), 759–808. <https://doi.org/10.1002/2016RG000529>
- Ismail Fawaz, H., Forestier, G., Weber, J., Idoumghar, L., & Muller, P. A. (2019). Deep learning for time series classification: A review. *Data Mining and Knowledge Discovery*, 33(4), 917–963. <https://doi.org/10.1007/s10618-019-00619-1>
- Kiranyaz, S., Avci, O., Abdeljaber, O., Ince, T., Gabbour, M., & Inman, D. J. (2021). 1D convolutional neural networks and applications: A survey. *Mechanical Systems and Signal Processing*, 151, 107398. <https://doi.org/10.1016/j.ymssp.2020.107398>
- Kiranyaz, S., Ince, T., & Gabbour, M. (2017). Personalized monitoring and advance warning system for cardiac arrhythmias. *Scientific Reports*, 7(1), 9270. <https://doi.org/10.1038/s41598-017-09544-z>
- Kreemer, C., Hammond, W. C., & Blewitt, G. (2018). A robust estimation of the 3-D intraplate deformation of the North American plate from GPS. *Journal of Geophysical Research: Solid Earth*, 123(5), 4388–4412. <https://doi.org/10.1029/2017JB015257>
- Larochelle, S., Chanard, K., Fleitout, L., Fortin, J., Gualandi, A., Longuevergne, L., et al. (2022). Understanding the geodetic signature of large aquifer systems: Example of the Ozark Plateaus in central United States. *Journal of Geophysical Research: Solid Earth*, 127(3), e2021JB023097. <https://doi.org/10.1029/2021JB023097>
- Li, Z., Lu, T., Yu, K., & Wang, J. (2023). Interpolation of GNSS position time series using GBDT, XGBoost, and RF machine learning algorithms and models error analysis. *Remote Sensing*, 2023, 15(18), 4374. <https://doi.org/10.3390/rs15184374>
- Özbey, V., Ergintav, S., & Tarı, E. (2024). GNSS time series analysis with machine learning algorithms: A case study for Anatolia. *Remote Sensing*, 16(17), 3309. <https://doi.org/10.3390/rs16173309>

- Peltier, W., Argus, D., & Drummond, R. (2015). Space geodesy constrains ice age terminal deglaciation: The global ICE6G_C (VM5a) model. *Journal of Geophysical Research: Solid Earth*, 120(1), 450–487. <https://doi.org/10.1002/2014JB011176>
- Rebischung, P., Villiger, A., Masoumi, S., & Herring, T. (2022). Upcoming switch to IGS20/igs20.atx and repro3 standards. IGSMAIL-8238. <https://lists.igs.org/pipermail/igsmailto/2022/008234.html>
- Rodgers, K. D., & Whaling, A. R. (2020). *Water levels and selected water-quality conditions in the Mississippi river Valley alluvial aquifer in eastern Arkansas, 2014*. U.S. Geological Survey Scientific Investigations Report 2020-5123, (p. 22). <https://doi.org/10.3133/sir20205123>
- Simonyan, K., & Zisserman, A. (2015). Very deep convolutional networks for large-scale image recognition. *arXiv:1409.1556*. <https://doi.org/10.48550/arXiv.1409.1556>
- Snay, R. A., Gillins, A. G., & Wang, G. (2025). Improving TRANS4D's crustal velocity model for the southeastern United States. *Journal of Surveying Engineering*, 151(4), 04025009. <https://doi.org/10.1061/JSUED2.SUENG-1572>
- Suito, H., & Freymueller, J. T. (2009). A viscoelastic and afterslip postseismic deformation model for the 1964 Alaska earthquake. *Journal of Geophysical Research*, 114(B11), 404. <https://doi.org/10.1029/2008JB005954>
- Taylor, J. P., Duncan, L. L., Leaf, A. T., Weisser, A. R., Dietsch, B. J., & Guira, M. (2024). *Inset groundwater-flow models for the cache and Grand Prairie critical groundwater areas, northeastern Arkansas*. U.S. Geological Survey Scientific Investigations Report 2024-5088, (p. 152). <https://doi.org/10.3133/sir20245088>
- Truong, C., Oudre, L., & Vayatis, N. (2020). Selective review of offline change point detection methods. *Signal Processing*, 167, 107299. <https://doi.org/10.1016/j.sigpro.2019.107299>
- Turco, M. J., Greuter, A., & Wang, G. (2025). A century (1906–2024) of groundwater and land subsidence studies in greater Houston region: A review. *Groundwater*, 63(4), 459–483. <https://doi.org/10.1111/gwat.70003>
- Wang, G. (2022). The 95% confidence interval for the GNSS-derived site velocities. *Journal of Surveying Engineering*, 148(1), 04021030. [https://doi.org/10.1061/\(ASCE\)SU.1943-5428.0000390](https://doi.org/10.1061/(ASCE)SU.1943-5428.0000390)
- Wang, G. (2023). A methodology for long-term offshore structural health monitoring using stand-alone GNSS: Case study in the Gulf of Mexico. *Structural Health Monitoring*, 23(1), 463–478. <https://doi.org/10.1177/14759217231169934>
- Wang, G., & Bao, Y. (2022). GNSS landslide monitoring aligned to regional reference frames. *Acta Geodaetica et Cartographica Sinica*, 51(10), 2107–2116. <https://doi.org/10.11947/J.AGCS.2022.20220308>
- Wang, G., Bao, Y., Cuddus, Y., Jia, X., Serna, J., & Jing, Q. (2015). A methodology to derive precise landslide displacement time series from continuous GPS observations in tectonically active and cold regions: A case study in Alaska. *Natural Hazards*, 77(3), 1939–1961. <https://doi.org/10.1007/s11069-015-1684-z>
- Wang, G., Bao, Y., Gan, W., Geng, J., Xiao, G., & Shen, S. (2018). NChina16, a stable geodetic reference frame for geological hazard studies in North China. *Journal of Geodynamics*, 115(Apr), 10–22. <https://doi.org/10.1016/j.jog.2018.01.003>
- Wang, G., Bao, Y., Zhang, S., Huang, G., & Hu, X. (2025). Python programs for training and implementing the ChangePointCNN-GNSS model. *Zenodo*. <https://doi.org/10.5281/zenodo.17180354>
- Wang, G., Boore, D. M., Tang, G., & Zhou, X. (2007). Comparisons of ground motions from colocated and closely spaced one-sample-per-second global positioning system and accelerograph recordings of the 2003 M 6.5 San Simeon, California, earthquake in the Parkfield region. *Bulletin of the Seismological Society of America*, 97(1B), 76–90. <https://doi.org/10.1785/0120060053>
- Wang, G., Greuter, A., Petersen, C. M., & Turco, M. J. (2022). Houston GNSS Network (HoustonNet) for subsidence and faulting monitoring: Data analysis methods and products. *Journal of Surveying Engineering*, 148(4), 04022008. [https://doi.org/10.1061/\(ASCE\)SU.1943-5428.0000399](https://doi.org/10.1061/(ASCE)SU.1943-5428.0000399)
- Wang, G., Liu, H., Mattioli, G. S., Miller, M. M., Feaux, K., & Braun, J. (2019). CARIB18: A stable geodetic reference frame for geological hazard monitoring in the Caribbean region. *Remote Sensing*, 11(6), 680. <https://doi.org/10.3390/rs11060680>
- Wang, G., Zhou, X., Wang, K., Ke, X., Zhang, Y., Zhao, R., & Bao, Y. (2020). GOM20, a stable geodetic reference frame for subsidence, faulting, and sea-level rise studies along the coast of the Gulf of Mexico. *Remote Sensing*, 12(3), 350. <https://doi.org/10.3390/rs12030350>
- Wang, J., Jiang, W., Li, Z., & Lu, Y. (2021). A new Multi-Scale Sliding Window LSTM Framework (MSSW-LSTM): A case study for GNSS time-series prediction. *Remote Sensing*, 13(16), 3328. <https://doi.org/10.3390/rs13163328>
- Welch, J., Wang, G., Bao, Y., Zhang, S., Huang, G., & Hu, X. (2024). Unveiling the hidden threat: Drought-induced inelastic subsidence in expansive soils. *Geophysical Research Letters*, 51(7), e2023GL107549. <https://doi.org/10.1029/2023GL107549>
- Xie, Y., Wang, J., Li, H., Dong, A., Kang, Y., Zhu, J., et al. (2023). Deep learning CNN-GRU method for GNSS deformation monitoring prediction. *Applied Sciences*, 14(10), 4004. <https://doi.org/10.3390/app14104004>
- Zhou, Y., Yang, S., Luo, J., Ray, J., Huang, Y., & Li, J. (2020). Global glacial isostatic adjustment constrained by GPS measurements: Spherical harmonic analyses of uplifts and geopotential variations. *Remote Sensing*, 12(7), 1209. <https://doi.org/10.3390/rs12071209>